ELSEVIER

Fluid Phase Equilibria 183–184 (2001) 331–339

FLUID PHASE EQUILIBRIA

www.elsevier.com/locate/fluid

Simulation of confined water in equilibrium with a bulk reservoir

I.V. Brovchenko [a], A. Geiger [a,*], D. Paschek [b]

[a] *Physikalische Chemie, Universitaet Dortmund, 44221 Dortmund, Germany*
[b] *Department of Chemical Engineering, University of Amsterdam, 1018 WV Amsterdam, The Netherlands*

Abstract

The properties of water in pores depend strongly on its average density, which is determined by the equilibrium with a bulk reservoir. In the present paper, Gibbs ensemble simulations were used for the equilibration of water in spherical pores with smooth surfaces and radii from 9 to 20 Å and bulk liquid water at $T = 300$ K and $P = 1$ bar.

The water density profile along the pore radius shows in all cases two prominent water layers near the pore surface. The oxygen–oxygen radial distribution functions evidence a clear distortion of the tetrahedral water structure in the first (outermost) layer towards a quasi-planar square- or hexagonal-like arrangement. An analysis of the non-short-circuited hydrogen-bond polygons evidences the existence of quasi-planar polygons in the first layer. Increasing the pore radius improves the water–water interaction between the two outer water layers, destroys the quasi-planar polygons and speeds up water diffusivity in the pore. The radial distribution functions of the hexagons evidence some distortion of the inner water in the pore towards the structure of cubic ice.

Keywords: Molecular simulation; Liquid–liquid equilibria; Water; Gibbs ensemble; Pores

1. Introduction

The thermodynamic equilibrium with a bulk reservoir determines the properties of liquids confined in pores. Hence, correct equilibration of the confined liquid with the bulk reservoir in molecular simulations is a necessary condition for a correct reproduction of its properties. Using Gibbs ensemble simulations [1] is the most direct and correct way for the equilibration of coexisting phases. This method was used recently for the simulation of water in spherical pores with radii R from 6 to 15 Å in equilibrium with bulk water at $T = 300$ K and $P = 1$ bar [2]. A vapour–liquid phase transition was observed at some strength of the water–pore interaction. Liquid water exists in such pores only when forming two prominent layers near the pore wall. The diffusivity of water in pores with $R = 12$ Å was found to be lower than in the bulk.

* Corresponding author. Tel.: +49-231-755-3937; fax: +49-231-755-3937.
E-mail address: geiger@pc2a.chemie.uni-dortmund.de (A. Geiger).

0378-3812/01/$20.00
PII: S0378-3812(01)00445-9

The effect of pore size and water–wall interaction in spherical pores with $R = 20$ Å is investigated in the present paper. The simulation of water in such large pores allows to investigate the properties of the inner water in the centre of the pore. This was practically impossible for the smaller pores due to the little amount of inner water. The local molecular structure of confined water is analyzed using distributions of non-short-circuited hydrogen bonded water polygons.

2. Simulation of water in spherical pores

TIP4P water [3] in spherical pores with radius $R = 20$ Å was simulated in equilibrium with bulk water at $T = 300$ K and $P = 1$ bar. The water–pore interaction was described by a (9–3) Lennard–Jones (LJ) potential, as a function of the distance between the oxygen atom and the wall [2]. The LJ-parameter σ in this potential was fixed to 2.5 Å. Two values of the LJ-parameter ε were used, leading to potentials with well-depths $U = -1.93$ and $U = -4.62$ kcal/mol ($U = -0.385\varepsilon$). The intermolecular interactions in the bulk water were calculated up to a cut-off distance of 12 Å, including long-range corrections for the Lennard–Jones part. The water–water interactions in the cavity were calculated without cut-off. The

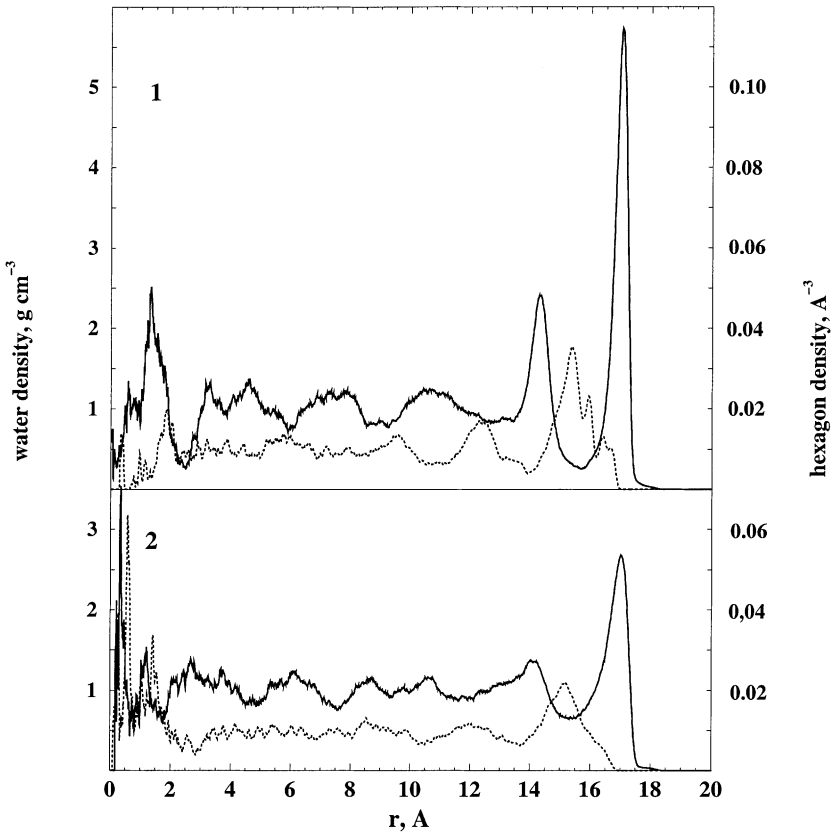

Fig. 1. Water density profile (solid line, left scale) and hexagon density profile (dotted line, right scale) along the pore radius: (1) $U = -4.62$ kcal/mol; (2) $U = -1.93$ kcal/mol.

equilibration with the bulk water was achieved by simulations in the Gibbs ensemble with essential numbers of molecular transfers between confined and bulk water [2]. The obtained average numbers of water molecules in the pore ($N_W = 852$ for $U = -1.93$ and $N_W = 952$ for $U = -4.62$ kcal/mol) were used in subsequent NVT ensemble MC and MD simulations to determine the structural and dynamic water properties.

An analysis of the distribution of non-short-circuited hydrogen bonded water rings was done following the procedure used in [4,5]. Two water molecules are considered as hydrogen bonded, when the distance between the oxygen does not exceed 3.5 Å and the pair interaction energy is lower than −2.25 kcal/mol.

3. Results

The variation of the water density along the pore radius is presented in Fig. 1. Two prominent water layers near the pore wall are observed in both systems. At the stronger water–pore interaction some

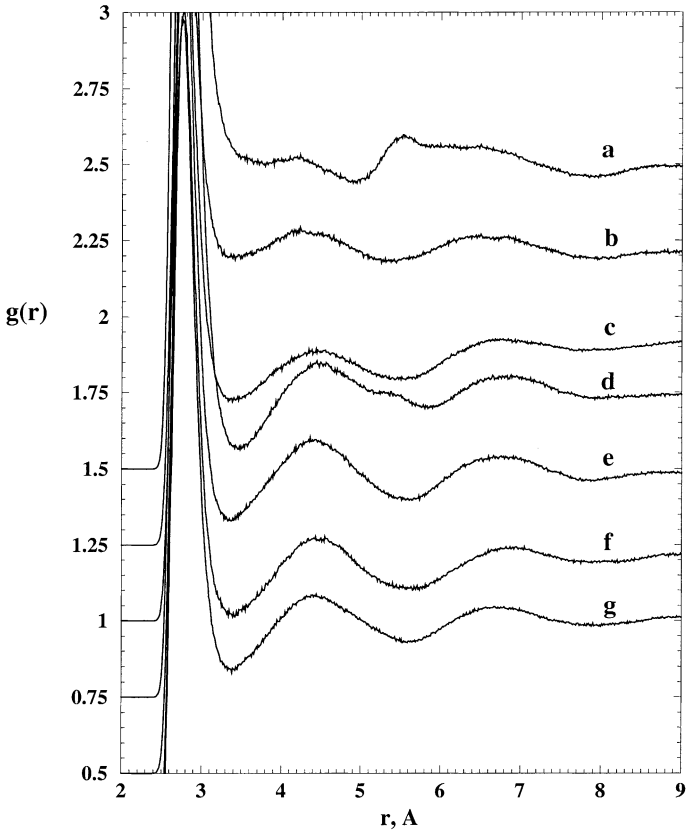

Fig. 2. Oxygen–oxygen RDFs for water in spherical pores (a–f, $R = 20$ Å) and bulk water (g); $U = -4.62$ kcal/mol (a–c). $U = -1.93$ kcal/mol (d–f); first outer layer (a and d), second layer (b and e), inner water (c and f); the curves are shifted successively by 0.25 in vertical direction.

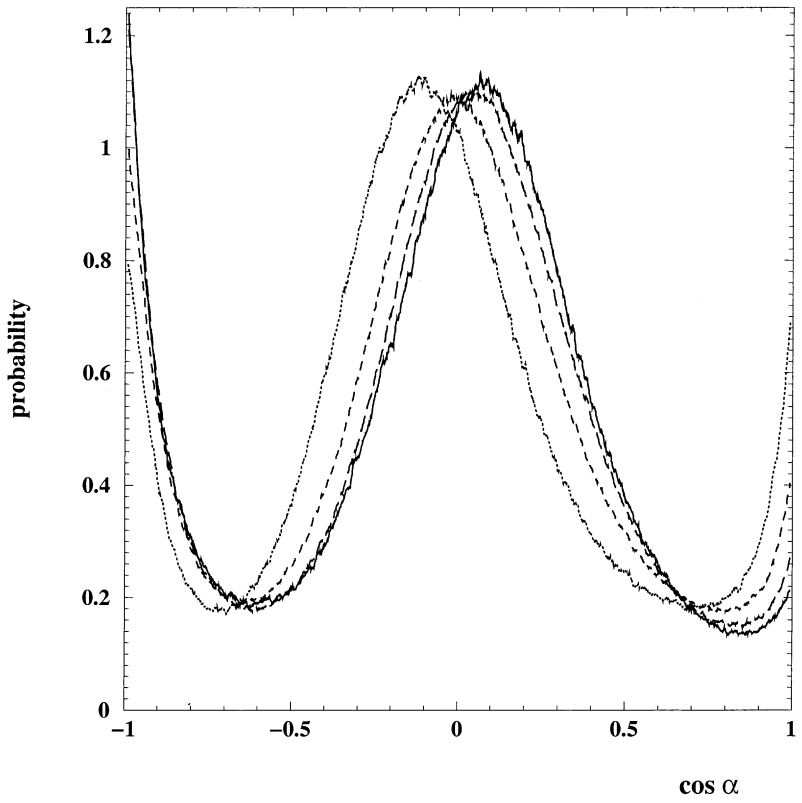

Fig. 3. Distribution of the angle α between the OH-vector and the pore radius vector for the water in the first outer layer ($U = -4.62$ kcal/mol): (dotted line) $R = 9$; (short-dashed line) $R = 12$; (long-dashed line) $R = 15$; (solid line) $R = 20$ Å.

additional layering of the inner water may be noted (Fig. 1). The large fluctuations of the density near the pore centre ($r < 3$ Å) reflect a worsening of the statistics due to the sharp decrease of the considered shell volumes. An analysis of the water properties was done for the first layer, second layer and the inner water separately. The location of the layers was determined by the minima in the local density $\rho(r)$ (Fig. 1).

When calculating the radial distribution functions (RDFs) the excluded volume effect due to the pore is taken into account. The RDFs which are attributed to a distinct water shell include distance correlations between pairs with at least one molecule belonging to this shell. The oxygen–oxygen RDFs $g_{OO}(r)$ of the inner water (Fig. 2c and f) and water in the second layer (Fig. 2b and e) are close to the bulk water (Fig. 2g). In contrast the tetrahedral water structure is sharply distorted in the first outer layer (Fig. 2a and d): the maximum at 4.4 Å which reflects the local tetrahedral structure decreases and an additional maximum appears at 5.5 Å. This effect becomes more pronounced with increasing water–pore interaction.

Angular distributions of the intramolecular OH vectors in the first water layer with respect to the pore radius vector are shown in Fig. 3 for different pore sizes and $U = -4.62$ kcal/mol. There are three main orientations of the OH-vectors: along the radius inwards ($\cos\alpha = -1$) and outwards ($\cos\alpha = +1$), and normal to the pore radius ($\cos\alpha = 0$). About 80% of the OH-vectors are oriented preferentially normal to the radius in all pores, whereas the probability to have orientations towards the pore centre increases

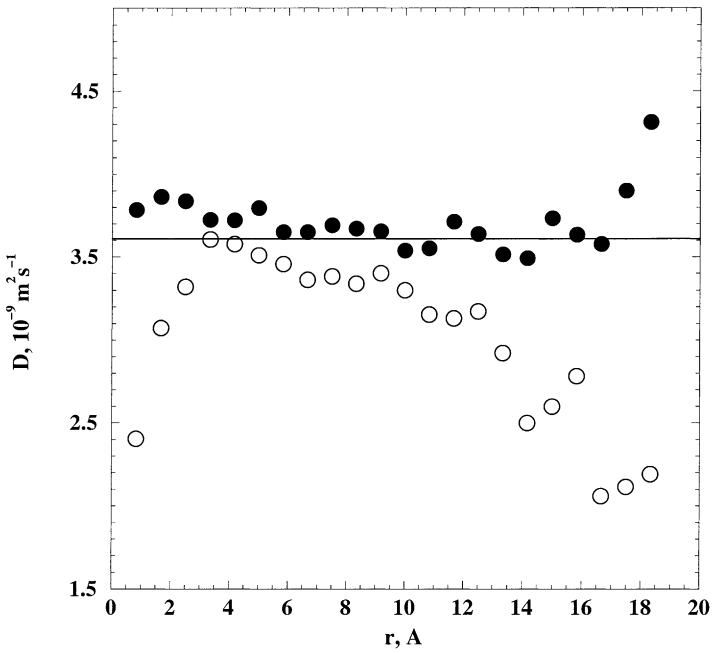

Fig. 4. Self-diffusion coefficient D of the water molecules which start at different distances r from the centre of the pore (pore radius $R = 20$ Å): (closed circles) $U = -1.93$; (open circles) $U = -4.62$ kcal/mol. The horizontal line corresponds to the bulk water value of D.

from 10 to 17% when the pore radius changes from 9 to 20 Å. This trend is also clearly seen from the distribution of the H atoms along the radius (not shown).

This increase of the number of OH-vectors in the first layer which are oriented towards the second water layer is accompanied by an increase of the average number of H-bonds. As a result, the total interaction energy per molecule in the first layer changes from −7.97 to −8.66 at $U = -4.62$ kcal/mol and from −7.64 to −8.43 at $U = -1.93$ kcal/mol, when the pore radius increases from 9 to 20 Å.

The dependence of the isotropic self-diffusion coefficient D on the location of the water molecules along the pore radius is shown in Fig. 4. Note the decrease of the water diffusivity near the surface in the pore with $U = -4.62$, whereas in the pore with $U = -1.93$ kcal/mol it is close to the bulk value. An increase of the pore size raises water diffusivity: the average value of the self-diffusion coefficient D increases from 1.85×10^{-9} to 2.59×10^{-9} m^2/s ($U = -4.62$ kcal/mol) and from 2.93×10^{-9} to 3.68×10^{-9} m^2/s ($U = -1.93$ kcal/mol), when the pore radius increases from 9 to 20 Å (the bulk value $D = 3.61 \times 10^{-9}$ m^2/s was obtained with the same parameters of interaction). For the determination of D in the confining pore, we refer to [2].

We also detected and analyzed the non-short-circuited hydrogen-bond rings of sizes $n = 3$–7. The general distribution of the centres of mass of the hexagons along the pore radius is presented in Fig. 1. A closer look to the distributions of the hexagons and pentagons in the region of the first water layer is shown in Figs. 5 and 6, respectively. A series of closely spaced but well resolved maxima can be observed. A geometrical analysis reveals, that the first density maxima in Figs. 5 (1) and 6 (1) correspond to rings of molecules which are all located in the first water layer. The next maximum represents hexagons with five

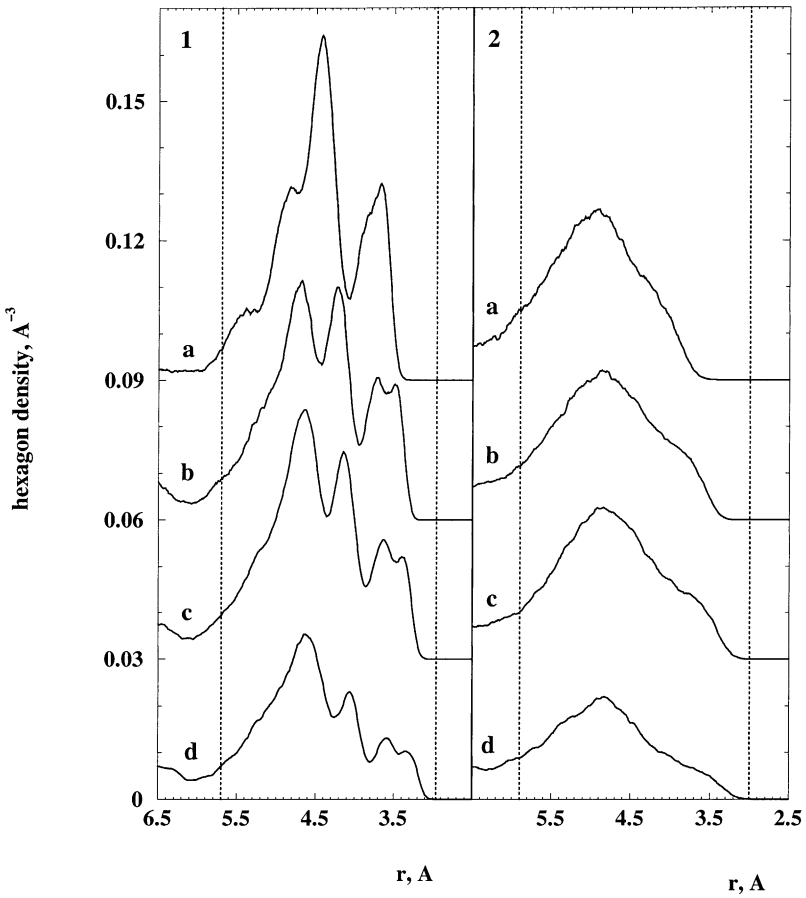

Fig. 5. Water hexagon density at distance r from the surface: (1) $U = -4.62$; (2) $U = -1.93$ kcal/mol; (a) $R = 9$; (b) $R = 12$; (c) $R = 15$; (d) $R = 20$ Å. Vertical dotted lines indicate positions of the water density maxima (see Fig. 1). The positions of the rings are identified by their centres of mass. The curves are shifted successively by 0.03 Å^{-3} in vertical direction.

oxygen in the first layer and one in the second layer and so on. In the pores with the weaker water–pore interaction the distribution of the polygons, which are located mainly in the first outer layer, is essentially lower and less structured (Figs. 5 (2) and 6 (2)).

The increase of the pore size allows the centres of mass of the hexagons and pentagons to be located closer to the surface, whereas the total density of the polygons in the outer layer decreases. Similar trends are observed for the polygons with sizes $n = 3$, 4 and 7.

The considerable volume of the inner water in the pores with $R = 20$ Å allows to investigate the RDF between the centres of the hexagons. The region up to 12.5 Å from the centre of the pore may be considered as inner water (see Fig. 1). To avoid correlations with the hexagons in the two water layers near the surface and to elucidate the excluded volume effect, the region in the centre of the pore up to 9 Å was analyzed. The RDFs of the centres of the hexagons are presented in Fig. 7 for water in the pore and bulk water. The RDFs for the hexagonal and cubic ices, which were obtained using available crystallographic data [6], are shown in the same figure. In general, the structure of the inner water is close to the bulk

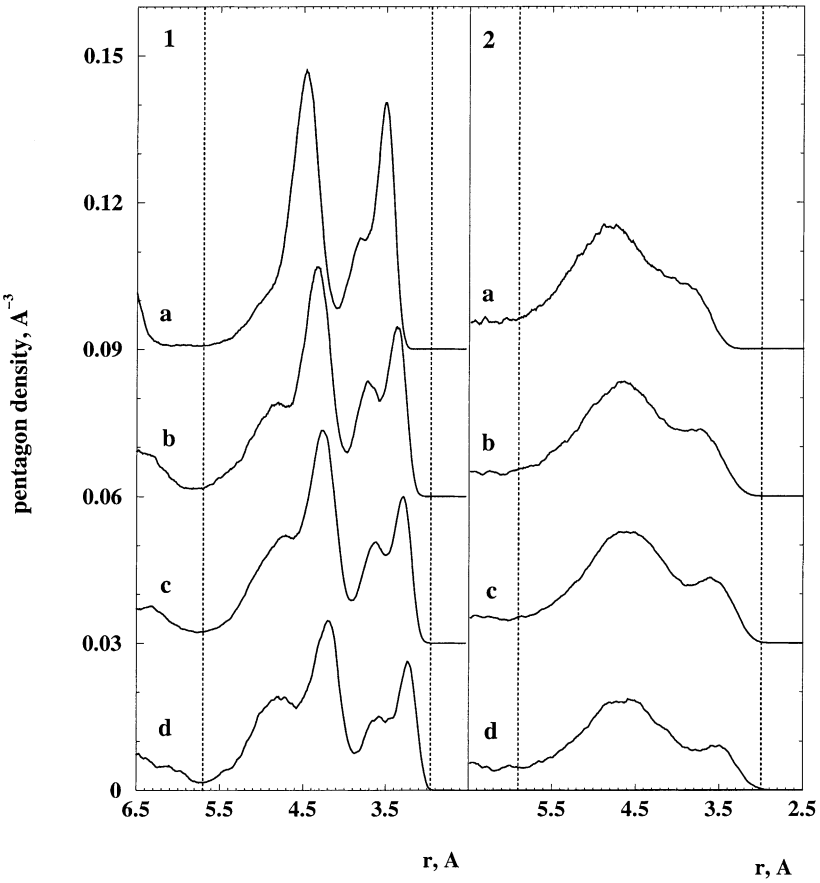

Fig. 6. Water pentagons density at distance r from the surface:(1) $U = -4.62$; (2) $U = -1.93$ kcal/mol; (a) $R = 9$; (b) $R = 12$; (c) $R = 15$; (d) $R = 20$ Å. Vertical dotted lines indicate positions of the water density maxima (see Fig. 1). The positions of the rings are identified by their centres of mass. The curves are shifted successively by 0.03 Å^{-3} in vertical direction.

water. A slight trend towards the structure of the cubic ice may be noted for the pore water: the maximum at 1.5 (in the more hydrophilic pore) and the maximum at 2.5 Å, observed for the hexagonal ice only, decrease, whereas the maximum at 2.3 Å, typical for the cubic ice, preserves its intensity.

4. Discussion

Our simulation of confined water in equilibrium with bulk water in the Gibbs ensemble gives the correct average water density in the pore. It allows to study the influence of pore sizes and water–pore interaction strength on the properties of the confined water.

Being in equilibrium with a bulk reservoir at ambient temperature and pressure, liquid water forms two layers near the wall of the spherical pores. Increase of the pore radius from 9 to 20 Å results in the appearance of a considerable volume of inner water in the centre of the pore, but the density profile of the two water layers near the wall does not change essentially [2] (Fig. 1).

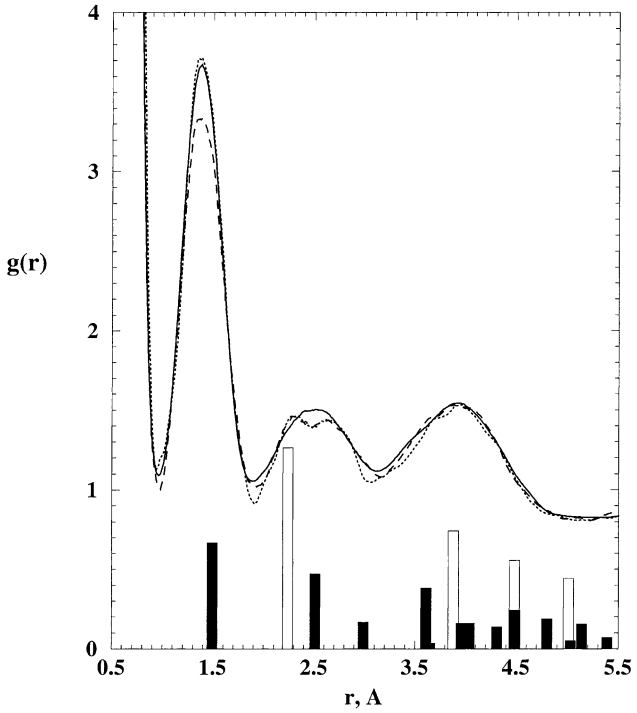

Fig. 7. RDF of the centres of the water hexagons: (solid line) bulk water; (dashed line) inner water in the pore with $U = -1.93$ kcal/mol, dotted line: inner water in pore with $U = -4.63$ kcal/mol. Bars correspond to the corresponding RDF in ice: (closed symbols) hexagonal ice; (open symbols) cubic ice.

Water diffusivity increases considerably with increasing pore size towards the bulk value [2] (Fig. 4). This is only partially connected with the increase of the total amount of the inner water, that has properties close to the bulk water. Increasing water diffusivity is also observed within the water layers near the wall and may be considered as the effect of the curvature of the surface on the water structure.

The water in the first layer is characterized by preferential orientation of the OH-vectors normal to the pore radius (Fig. 3). The flattening of the surface does not effect this preferential orientation, but makes more OH-vectors to be oriented towards the pore centre instead of an outward orientation. This is reflected in the angular distribution of the OH-vectors (Fig. 3) and density distribution of the H atoms along the pore radius. As a result, the average number of H-bonds increases and the water–water interaction becomes stronger in the first layer. By this the connection between the first water layer and the rest of the water becomes more bulk-like and the diffusivity of the water molecules increases.

The additional maximum in the RDF $g_{OO}(r)$ around 5.5 Å observed for the first water layer (Fig. 2) is the characteristic feature of a quasi-planar water structure. This maximum corresponds to the doubling of the first maximum of $g_{OO}(r)$ at 2.75 Å and reflects the appearance of a quasi-planar square-like or hexagonal-like arrangement of water oxygen in the first layer.

An analysis of the non-short-circuited water rings was used to get additional information on the local molecular order of the confined water. The existence of quasi-planar hydrogen bonded water polygons of different sizes in the first water layer are indicated by those peaks in Figs. 5 and 6, which belong to rings

with a centre of mass close to the surface. This shows a similarity between the water structure on the pore surface and the structure of clathrate-like cages which are formed around solute molecules in water [7,8]. Strengthening the water–pore interaction and decreasing the pore size improves the clathrate-like character of the water structure in the first layer.

The RDFs of the water hexagons in the central part of the pore show, that due to the confinement the structure of water becomes closer to the cubic ice structure. This agrees with the experimentally observed freezing of confined water into cubic ice [9,10].

5. Conclusions

The effect of pore size and water–pore interaction strength on the properties of the confined water is analyzed for spherical pores with smooth surface. Spherical confinement promotes the appearance of a quasi-planar water layer near the surface, which shows some feature of a clathrate-like structure. Flattening of the pore surface destroys the quasi-planar water structure on the surface and increases water diffusivity in the pore.

Acknowledgements

Support from the Graduiertenkolleg Struktur-Dynamik Beziehungen in mikrostrukturierten Systemen and from Fonds der Chemischen Industrie is gratefully acknowledged.

References

[1] A.Z. Panagiotopoulos, Mol. Phys. 62 (1987) 701–719.
[2] I. Brovchenko, D. Paschek, A. Geiger, J. Chem. Phys. 113 (2000) 5026–5036.
[3] W.L. Jorgensen, J. Chandrasekhar, J.D. Madura, J. Chem. Phys. 79 (1983) 926–936.
[4] A. Rahman, F. H Stillinger, J. Am. Chem. Soc. 95 (1973) 7943–7948.
[5] P. Mausbach, J. Schnitker, A. Geiger, J. Tech. Phys. 28 (1987) 67–76.
[6] R.W. Grove, D.P. Santry, Chem. Phys. 2 (1973) 304–320.
[7] A. Geiger, A. Rahman, R.W. Stillinger, J. Chem. PhDs 70 (1979) 263–276.
[8] B. Guillot, Y. Guissani, J. Chem. Phys. 99 (1993) 8075–8094.
[9] M.-C. Bellissent-Funel, J. Lal, L. Bosio, J. Chem. Phys. 98 (1993) 4246–4252.
[10] L.J. Barbour, G.W. Orr, J.L. Atwood, Nature 393 (1998) 671–673.